Supplement of Atmos. Meas. Tech., 10, 4877–4894, 2017
https://doi.org/10.5194/amt-10-4877-2017-supplement

Atmospheric Measurement Techniques
Open Access
EGU

Supplement of

An intercomparison of HO_2 measurements by fluorescence assay by gas expansion and cavity ring-down spectroscopy within HIRAC (Highly Instrumented Reactor for Atmospheric Chemistry)

Lavinia Onel et al.

Correspondence to: Lavinia Onel (chmlo@leeds.ac.uk), Paul W. Seakins (p.w.seakins@leeds.ac.uk), Grant A. D. Ritchie (grant.ritchie@chem.ox.ac.uk), and Dwayne E. Heard (d.e.heard@leeds.ac.uk)

S1 FAGE calibration for HO_2 at atmospheric pressure using H_2O vapour photolysis

Figure S1 shows an example of FAGE calibration plot obtained by using the photolysis of water at 185 nm in air to generate known concentrations HO_2. The average calibration constant was:

$C_{HO2} = (2.6 \pm 0.4) \times 10^{-7}$ counts cm^3 $molecule^{-1}$ s^{-1} mW^{-1},

where the error is a combination of systematic and statistical uncertainties at the 1σ level.

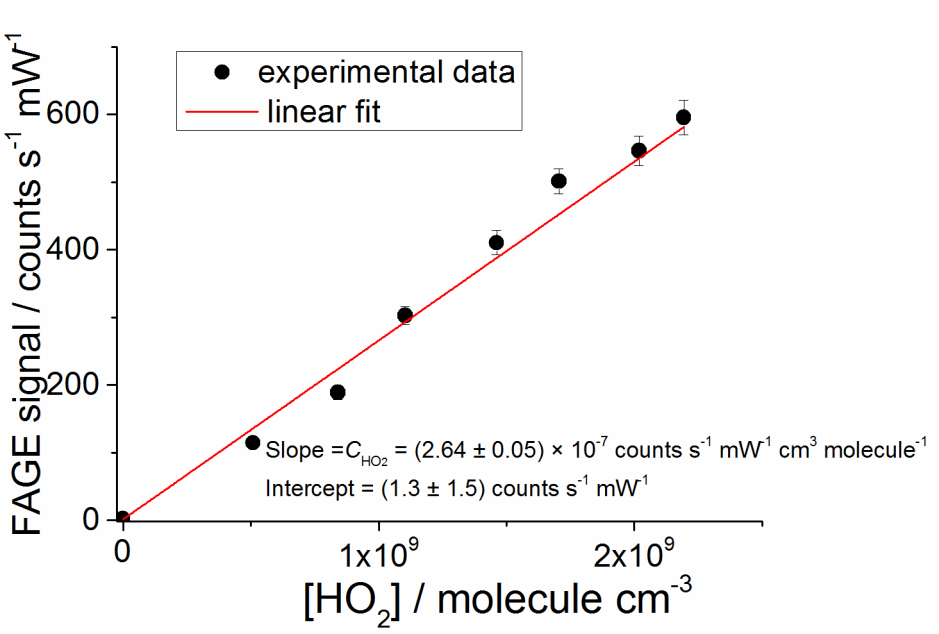

Figure S1. FAGE calibration for HO_2 at atmospheric pressure and 293 K; laser power = (3.7 ± 0.1) mW; pressure in the detection cell = (3.24 ± 0.20) mbar. The FAGE signal, including the measurement with the Hg lamp turned off ($[HO_2] = 0$), was obtained by subtraction of the online signal in the absence of NO from the signal in the presence of NO (~ 6×10^{13} molecule cm^{-3}). Averaging time per point = 120 s. The error limits in [HO2] and the FAGE signal are representative for the 1σ statistical uncertainty.

S2 Kinetics of the FAGE HO_2 signal temporal decay at 1000 mbar

The kinetics of the temporal decay of the fluorescence HO_2 signal at 1000 mbar monitored by FAGE when HIRAC UV lamps were extinguished has been used to determine the FAGE calibration factor, C_{HO2}, in order to compare it with C_{HO2} obtained by using the water photolysis method (Sect. S1). Eight determinations (Table S1) have been carried out using Eq. (S1) (Eq. (4) in the main text):

$$(S_{HO_2})_t = \left(\left(\frac{1}{(S_{HO_2})_0} + \frac{2 \cdot k_{self\text{-}r.}}{k_{loss} \cdot C_{HO_2}} \right) \times \exp(k_{loss} t) - \left(\frac{2 \cdot k_{self\text{-}r.}}{k_{loss} \cdot C_{HO_2}} \right) \right)^{-1}, \qquad \text{(S1)}$$

where $(S_{HO2})_t$ is the fluorescence signal at reaction time t, $(S_{HO2})_0$ is the signal at time $t = 0$, when the lamps were turned off, $k_{self\text{-}r.}$ is the overall HO_2 self-reaction rate coefficient, i.e. the sum of the bimolecular rate coefficient of Reaction (R1) and the termolecular rate coefficient of Reaction (R2) at 1000 mbar of air, and k_{loss} is the rate coefficient describing the HO_2 wall-loss.

$$HO_2 + HO_2 \rightarrow H_2O_2 + O_2 \quad \text{(R1)}$$

$$HO_2 + HO_2 + M \rightarrow H_2O_2 + O_2 + M \qquad (M = N_2 \text{ or } O_2) \quad \text{(R2)}$$

$$HO_2 \rightarrow \text{loss} \quad \text{(R3)}$$

The average value of the eight independent determinations was:

$C_{HO2} = (2.4 \pm 0.5) \times 10^{-7}$ counts cm^3 molecule^{-1} s^{-1} mW^{-1},

where the error is the overall uncertainty obtained by combining the systematic and statistical uncertainties at the 1σ level.

Table S1. FAGE calibration factor for HO_2, C_{HO2}, and the rate coefficient of the HO_2 wall-loss within HIRAC, k_{loss}, at 1000 mbar extracted by fitting Eq. (S1) to the temporal decays of the FAGE signal, S_{HO2}. The initial HO_2 concentration was then computed by using: $[HO_2]_0 = (S_{HO2})_0 / C_{HO2}$ to obtain values between 0.8–1.1 × 10^{11} molecule cm^{-3}.

$10^7 \times C_{HO2}$[a] / counts s^{-1} mW^{-1} cm^3 molecule^{-1}	**k_{loss} / s^{-1}**
2.00 ± 0.01	0.048 ± 0.001
2.13 ± 0.01	0.038 ± 0.001
2.34 ± 0.01	0.047 ± 0.001
2.30 ± 0.03	0.045 ± 0.002
2.07 ± 0.02	0.038 ± 0.002
3.01 ± 0.05	0.062 ± 0.002
2.50 ± 0.02	0.028 ± 0.001
2.78 ± 0.03	0.044 ± 0.002

[a] statistical uncertainties quoted to 1σ

S3 Kinetics of the FAGE HO_2 signal temporal decay at 150 mbar

The FAGE calibration factor for HO_2 at 150 mbar was determined by the kinetic method presented above for 1000 mbar, by fitting Eq. (S1) (Eq. (4) in the main paper) to the temporal decays of the HO_2 FAGE signal generated in HIRAC when the UV lamps were turned off. Nine determinations (Fig. 2 in the main text shows an example) were performed in total with the average result:

$C_{HO2} = (2.6 \pm 0.5) \times 10^{-7}$ counts cm^3 $molecule^{-1}$ s^{-1} mW^{-1},

where the error represent the overall 1σ uncertainty.

Table S2. FAGE calibration factor for HO_2, C_{HO2}, and the rate coefficient of the HO_2 wall-loss within HIRAC, k_{loss}, at 150 mbar extracted by fitting Eq. (S1) to the temporal decays of the FAGE signal, S_{HO2}. The initial HO_2 concentration was then computed by using: $[HO_2]_0 = (S_{HO2})_0 / C_{HO2}$ to obtain values between 0.5–1.1 × 10^{11} molecule cm^{-3}.

$10^7 \times C_{HO2}$[a] / counts s^{-1} mW^{-1} cm^3 $molecule^{-1}$	k_{loss} / s^{-1}
2.30 ± 0.02	0.079 ± 0.007
2.64 ± 0.01	0.099 ± 0.003
2.29 ± 0.08	0.088 ± 0.004
2.85 ± 0.05	0.093 ± 0.002
3.04 ± 0.02	0.103 ± 0.005
2.71 ± 0.07	0.084 ± 0.002
2.69 ± 0.05	0.083 ± 0.002
2.48 ± 0.07	0.088 ± 0.002
2.41 ± 0.12	0.051 ± 0.005

[a] statistical uncertainties quoted to 1σ

S4 Calibration of the distributed feedback (DFB) diode laser

The current to the DFB diode laser (NTT Electronics, NLK1S5GAAA) and the built-in thermoelectric element as well as the thermistor temperature have been controlled by a Thorlabs ITC502 driver. The laser has been calibrated using a wavemeter (Burleigh WA-1000) at the operating current of 130 mA. Figure S2 shows an example of the calibration plot.

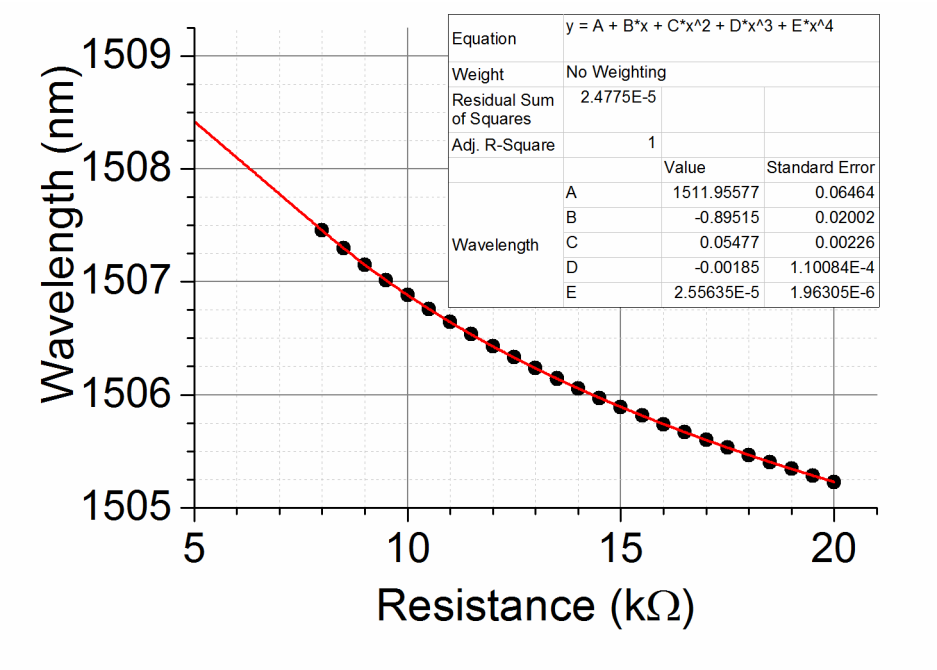

Figure S2. Emission wavelength vs. thermistor resistance used as calibration plot of the DFB diode laser for a current of 130 mA. The resistance of the built-in thermoelectric element is changed by varying its temperature.

During experiments the resistance is measured and the graph above used to generate the laser wavelength.

S5 Water vapour absorption spectra

The absorption lines of water vapour nearby the region of interest for CRDS HO_2 measurements have been recorded to demonstrate the ability of the CRDS system to reproduce the position of the water vapour line-centres and their relative strengths as reported in the High-resolution transmission molecular absorption (HITRAN) database (Richard et al., 2012). The water vapour absorption spectrum between 1506.2 – 1506.8 nm at 150 and 1000 mbar of air have been compared to the spectra reported in HITRAN at the same pressures, and very good agreement is found, as shown Fig. S3. Almost all the five spectral features found at 150 mbar represent single absorption lines (Richard et al., 2012). At 1000 mbar the weaker spectral features, centred at 1506.66 nm and 1506.51 nm are in the noise, while the line centred at 1506.35 nm overlaps with the one at 1506.27 nm due to the pressure broadening by air.

The H_2O vapour concentrations corresponding to the measurement at 150 mbar and 1000 mbar shown by the red lines in Fig. S3a and Fig. S3b, were ~ 1.5×10^{15} molecule cm^{-3} and ~ 7.5×10^{14}

molecule cm^{-3}, respectively, and were achieved by injecting H_2O in the liquid phase into a stream of N_2 which was then delivered to HIRAC, which had previously been filled with synthetic air. The delivered [H_2O_{vapour}] was determined from FTIR measurements (Sect. S8) performed a few minutes after the H_2O delivery to allow for the mixing within the chamber. At both pressures under typical HIRAC background conditions, i.e. without adding water to the chamber, H_2O vapour was present at concentrations of 10^{13}–10^{14} molecule cm^{-3}.

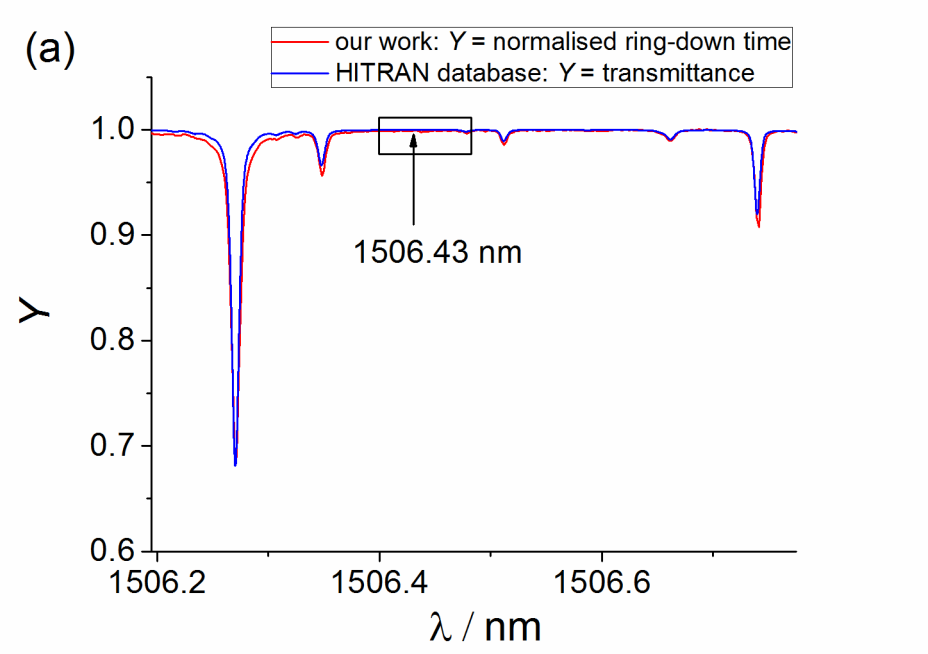

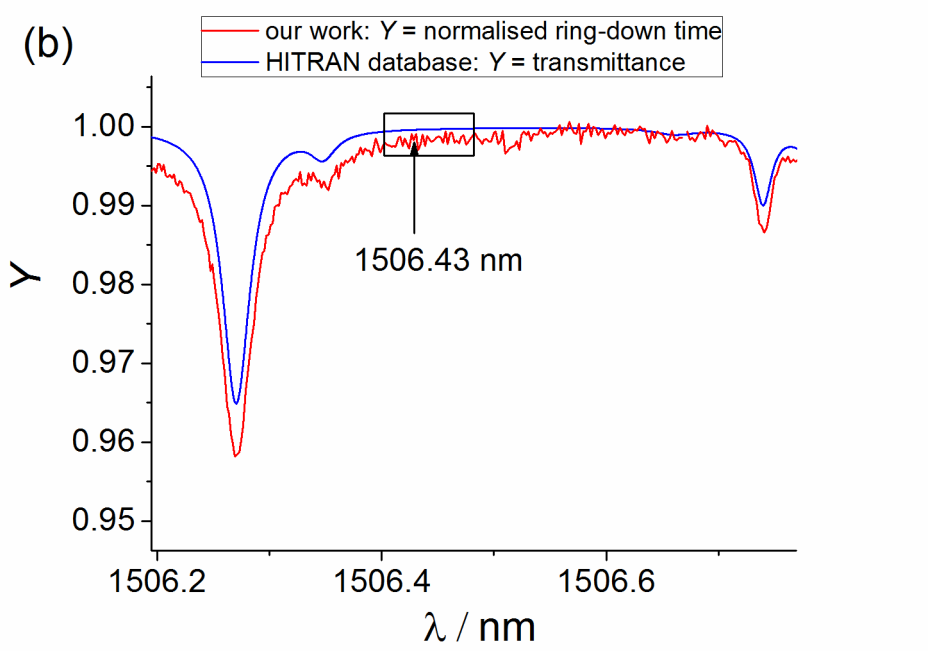

Figure S3. Water vapour spectrum at (a) 150 mbar and (b) 1000 mbar total pressure of synthetic air recorded inside HIRAC. The experimental concentration of H_2O is ~ 1.5 × 10^{15} molecule cm^{-3} (150 mbar) and ~ 7.5 × 10^{14} molecule cm^{-3} (1000 mbar), calibrated using FTIR spectroscopy inside HIRAC. The red line represents the recorded ring-down time (τ) divided by $\tau_{1506.6\ nm}$ and the blue line is the transmission spectrum of H_2O computed using HITRAN (Richard et al., 2012) for the experimental [H_2O] at each operating pressure. The arrow is pointing to the value of 1506.43 nm, which was used in all the fixed wavelength measurements for HO_2 detection, while the black rectangle shows the wavelength range scanned to find the spectral features of HO_2 shown in the experimental section in the main paper (Fig. 3).

S6 Comparison of the CRDS measurements with the HIRAC fans on to the measurements with the fans off

The ring-down time was recorded continuously in the absence of HO_2 under constant conditions (T = 295 K, p = 1000 mbar of synthetic air) and maintaining the HIRAC fans on and off, respectively, for a period of ~ 1.2 hours, as shown in Fig. S4a. The generated Allan deviation plots (Fig. S4b) show that for a signal-to-noise ratio (S/N) of 2, the minimum detectible absorption coefficient corresponding to a single ring-down measurement is α_0 = 7.2 × 10^{-10} cm^{-1} if the fans are on, which reduces to α_0 = 4.8 × 10^{-10} cm^{-1} if the fans are off. For S/N = 2, the best CRDS sensitivity is achieved by averaging ~ 600 ring-down events (requiring 60 s at an acquisition rate of 10 Hz) and giving a minimum absorption coefficient of α_0 = 5.4 × 10^{-11} cm^{-1} when the fans are on and α_0 = 4.0 × 10^{-11} cm^{-1} when the fans are not in use.

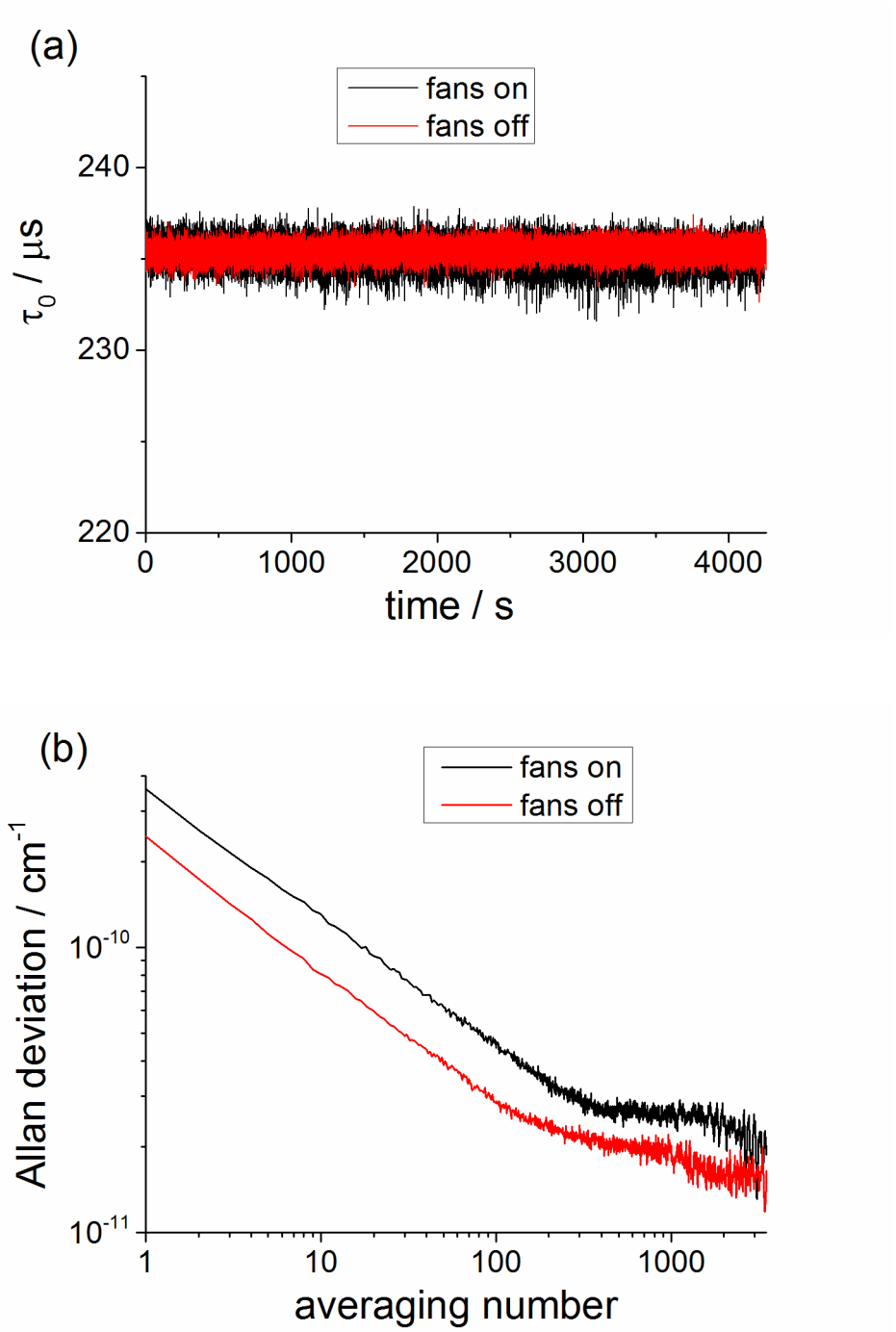

Figure S4. (a) Measurement of the single ring-down events at 1000 mbar of air maintaining the chamber fans on (black line) and off (red line) during ~ 1.2 hours of measurements, and (b) the corresponding Allan deviation plots of the absorption coefficient at 1506.43 nm vs. the number of ring-down events averaged.

S7 Determination of σ_{CH3OH} and σ_{CH2O} in the ~ 1506.4–1506.5 nm wavelength range

The absorption cross-section of CH_3OH at 1506.43 nm, σ_{CH3OH}, has been determined at both HIRAC operating pressures (150 mbar and 1000 mbar) by measuring the ring-down time at 1506.43 nm, τ, before and after delivering known concentrations of CH_3OH to the chamber. The absorption coefficient at 1506.43 nm, α, was computed using Eq. (S2).

$$\alpha = \frac{1}{c}\left(\frac{1}{\tau} - \frac{1}{\tau_0}\right), \qquad \text{(S2)}$$

Here τ_0 is the ring-down time before adding CH_3OH to HIRAC, which has been filled with synthetic air at 150 mbar and 1000 mbar, respectively. As $\sigma_{CH3OH} = \frac{\alpha}{[CH3OH]}$, σ_{CH3OH} was obtained as the gradient of the linear fit of α vs. $[CH_3OH]$ (Fig. S5) where the intercept was fixed to zero. Figure S6 shows laser wavelength scans at the two chamber pressures, τ vs. λ, performed over the wavelength range of interest, ~1506.39–1506.48 nm, after delivering CH_3OH in typical concentrations. The CH_3OH addition produced a decrease in the ring-down time: $(\Delta\tau/\tau_0)_{150\ mbar} \cong 0.05$ and $(\Delta\tau/\tau_0)_{1000\ mbar} \cong 0.10$. At both pressures the CH_3OH absorption is practically constant across all the scanned wavelength range.

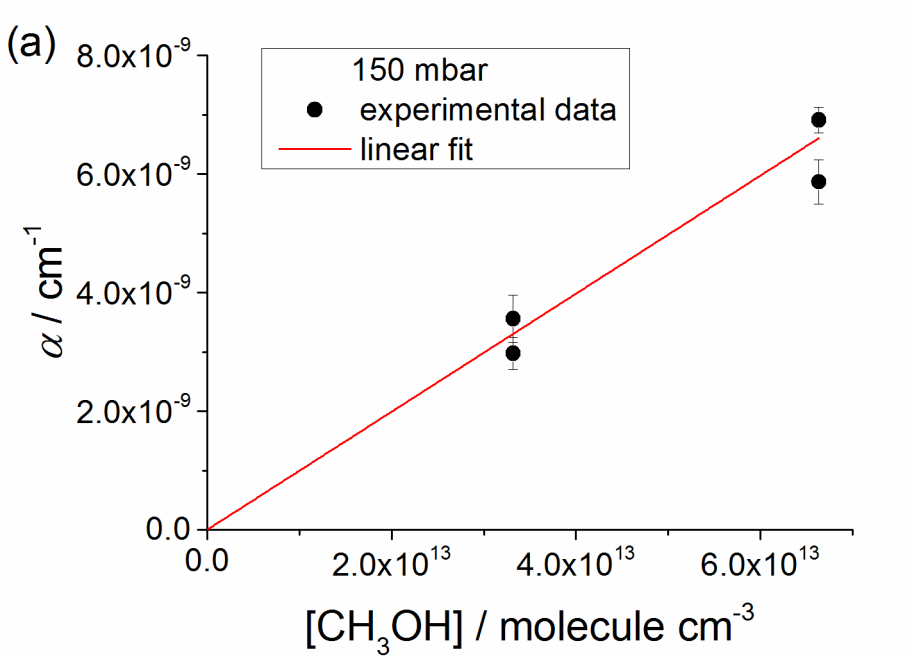

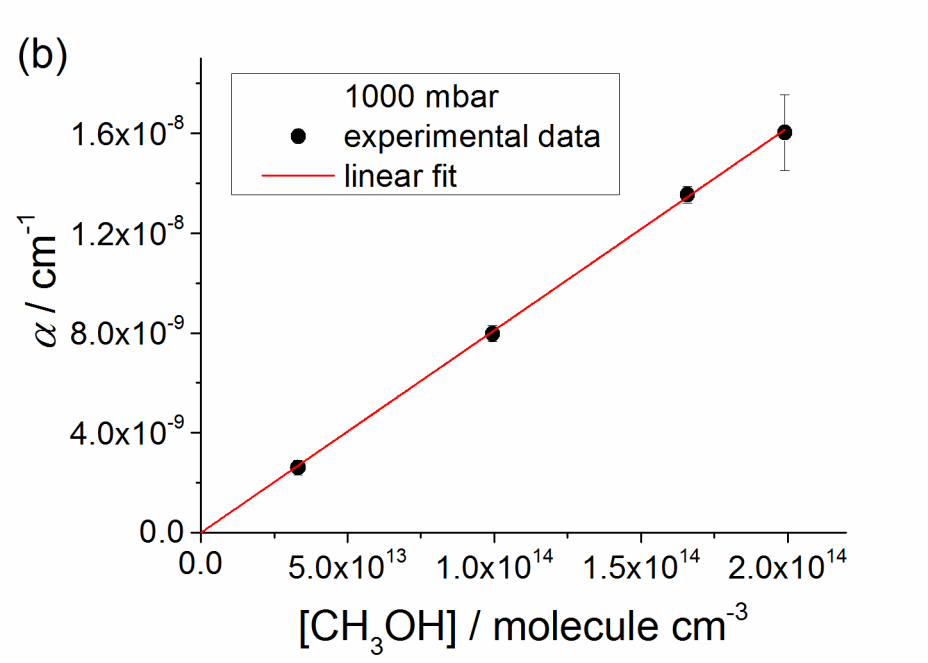

Figure S5. Absorption coefficient at 1506.43 nm, α, as a function of CH_3OH concentration at (a) 150 mbar and (b) 1000 mbar.. The gradient of the linear fit (red line) represents the CH_3OH cross section at 1506.43 nm: $\sigma_{CH3OH,\ 150\ mbar}$ = (9.95 ± 0.42) × 10^{-23} cm^2 molecule and $\sigma_{CH3OH,\ 1000\ mbar}$ = (8.11 ± 0.05) × 10^{-23} cm^2 $molecule^{-1}$ (statistical error at 1sigma level).

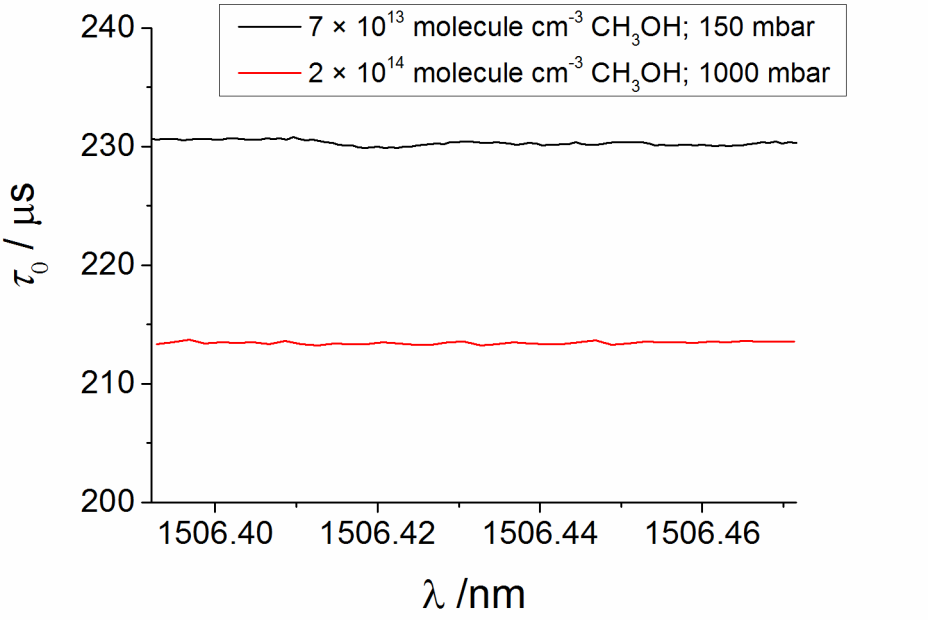

Figure S6. Ring down-time, τ, after delivering CH_3OH to HIRAC as a function of wavelength in the range of the scanned HO_2 absorption feature (Fig. 3 in the main manuscript) at the two applied pressures: $[CH_3OH]_0$ = 7 × 10^{13} molecule cm^{-3}; 150 mbar (black line) and $[CH_3OH]_0$ = 2 × 10^{14} molecule cm^{-3}; 1000 mbar (red line).

In addition, a few measurements of the decrease in the ring-down time when CH_2O was delivered in known concentrations to the chamber have been performed to estimate that the absorption cross section of CH_2O at 1506.43 nm is ~ 3×10^{-23} cm^2 $molecule^{-1}$ on average at both 150 mbar and 1000 mbar. This estimated σ_{CH2O} is a few times lower than the reported value (Ruth et al., 2015) obtained using 2 mbar of pure CH_2O, and can be rationalised by the air-broadening in the present measurements.

S8 FTIR measurements

CH_3OH was detected during the experiments using *in situ* multi-pass FTIR along the long axis of HIRAC. The multi-pass Chernin arrangement within the chamber was optimised for 72 internal reflections giving an approximate total path length of 128.5 m (Glowacki et al., 2007;Winiberg et al., 2016). IR spectra were recorded every half a minute as the average of 30 scans (30 s integration time) at 1 cm^{-1} resolution. [CH_3OH] during the experiments was obtained using the absorption at ~ 1030 cm^{-1} due to the C-O stretch by using reference spectra at 150 and 1000 mbar taken of methanol delivered in known concentrations to the chamber. Two methods of delivery were used: (i) injecting a known volume of liquid CH_3OH in a N_2 stream delivered to HIRAC and (ii) delivering CH_3OH vapour at a known pressure to a one litre stainless steel cylinder followed by the delivery of the CH_3OH from the cylinder to the chamber using a flow of N_2. A virtually identical CH_3OH absorption spectrum in the range 700–4000 cm^{-1} was measured when the same amount of CH_3OH was delivered to HIRAC using separately the two methods.

S9 Determination of σ_{HO2}(1506.43 nm)

S9.1 σ_{HO2}(1506.43 nm) vs. pressure between 0–1100 mbar of air

The cross section of HO_2 at 1506.43 nm in the range 0–1100 mbar of air was computed by using a model which takes into account the line centred at 1506.43 nm together with the contribution of the neighbouring transitions, due to the air-broadening of the absorption lines (details in Sect. 3.2 in the main text). The simplest equation that fits well the obtained data, σ_{HO2} as a function of pressure, was:

$$\sigma_{HO2} = A_0 + A_1 \exp(-\lambda_1 p) + A_2 \exp(-\lambda_2 p). \quad \text{(S3)}$$

The values of the fit parameters, A_0, A_1, A_2, λ_1 and λ_2 are given in Table S3.

Table S3. Parameters generated by fitting Eq. (S3) to σ_{HO2}(1506.43 nm) vs. pressure (in mbar) computed by application of pressure broadening to the spectral lines reported by Thiebaud et al. (2017).

$\sigma_{HO2} = A_0 + A_1\exp(-\lambda_1 p) + A_2\exp(-\lambda_2 p)$		
A_0	$(2.88 \pm 0.04) \times 10^{-20}$	cm^2 molecule^{-1}
A_1	$(2.91 \pm 0.04) \times 10^{-19}$	cm^2 molecule^{-1}
λ_1	$(1.36 \pm 0.04) \times 10^{-2}$	mbar^{-1}
A_2	$(8.87 \pm 0.34) \times 10^{-20}$	cm^2 molecule^{-1}
λ_2	$(2.76 \pm 0.1) \times 10^{-3}$	mbar^{-1}

S9.2 σ_{HO2}(1506.43 nm) at 150 mbar using the kinetics of the HO_2 temporal decay

The kinetics of the temporal decay monitored by CRDS when HIRAC UV lamps were turned off, i.e. HO_2 absorption coefficient at 1506.43 nm (α_{HO2}) vs. time, has been used to determine σ_{HO2} at 150 mbar. The absorption coefficient α_{HO2} was computed using Eq. (S4) (Eq. (9)).

$$\alpha_{HO_2} = \frac{1}{c}\left(\frac{1}{\tau} - \frac{1}{\tau_0}\right), \qquad \text{(S4)}$$

σ_{HO2} was obtained by fitting Eq. (S5) (Eq. (10)) in the main paper) to the experimental temporal decays of α_{HO2}.

$$(\alpha_{HO_2})_t = \left(\left(\frac{1}{(\alpha_{HO_2})_0} + \frac{2 \cdot k_{\text{self-r.}}}{k_{loss} \cdot \sigma_{HO_2}}\right) \times \exp(k_{loss} t) - \left(\frac{2 \cdot k_{\text{self-r.}}}{k_{loss} \cdot \sigma_{HO_2}}\right)\right)^{-1}, \qquad \text{(S5)}$$

where $(\alpha_{HO2})_t$ and $(\alpha_{HO2})_0$ are the absorption coefficient at time t and $t = 0$ (the time when the UV lamps were extinguished), $k_{\text{self-r.}} = 1.79 \times 10^{-12}$ cm^{-3} molecule^{-1} s^{-1} is the overall HO_2 self-reaction rate coefficient, i.e. the sum of the bimolecular rate coefficient of Reaction (R1) and the termolecular rate coefficient of Reaction (R2) at 150 mbar of air, and k_{loss} is the rate coefficient describing the HO_2 wall-loss (Reaction (R3)).

A total of eight independent determinations were performed with the results presented in Table S4; the average results are: $\sigma_{HO2} = (1.02 \pm 0.18) \times 10^{-19}$ cm^2 molecule^{-1} and $k_{loss} = (0.11 \pm 0.01)$ s^{-1} (the error

limits represent overall errors at 1σ level). The σ_{HO2} value is 23% lower than the σ_{HO2} determined using previous reported spectral data for HO_2, $(1.25 \pm 0.19) \times 10^{-19}$ cm^2 molecule^{-1}. However, the two values have overlapping error limits.

Table S4. σ_{HO2}(1506.43 nm) and the rate coefficient of the HO_2 wall-loss within HIRAC, k_{loss}, extracted by fitting Eq. (S5) to the experimentally recorded α_{HO2} vs. time data at 150 mbar. α_{HO2} was computed using Eq. (S4).

$10^{19} \times \sigma_{HO2}$[a] / cm^2 molecule^{-1}	k_{loss} / s^{-1}
1.02 ± 0.03[b]	0.109 ± 0.004
0.98 ± 0.01[b]	0.105 ± 0.003
1.01 ± 0.01[b]	0.110 ± 0.003
1.01 ± 0.02[b]	0.105 ± 0.004
1.02 ± 0.01[b]	0.108 ± 0.003
1.06 ± 0.04[c]	0.120 ± 0.006
1.02 ± 0.05[c]	0.110 ± 0.005
1.07 ± 0.07[c]	0.109 ± 0.006

[a] uncertainties quoted to 1σ
[b] $[HO_2]_0 = (1.03 \pm 0.04) \times 10^{11}$ molecule cm^{-3} (obtained by using: $[HO_2]_0 = (\alpha_{HO2})_0 / \sigma_{HO2}$)
[c] $[HO_2]_0 = (4.72 \pm 0.04) \times 10^{10}$ molecule cm^{-3} (computed by using: $[HO_2]_0 = (\alpha_{HO2})_0 / \sigma_{HO2}$)

As the cavity mirrors are mounted 100 mm from the chamber internal wall, $[HO_2]$ is expected to be lower along the 100 mm distance before each mirror compared to $[HO_2]_{HIRAC}$. Investigations have been carried out to test the sensitivity of the results shown in Table S4 to the approximation that $[HO_2]$ is homogeneous across the entire cavity length (the distance between the mirrors), L = 1400 mm. The absorption coefficient has been re-computed by considering that HO_2 is absent in the systems of flanges connecting the mirrors to the chamber (14% of L). In this worst-case scenario, the absorption coefficient is higher by a factor equal to the ratio between L and the HIRAC diameter, where HO_2 is present, L_{HO2} (1200 mm):

$$\alpha_{HO_2} = \frac{L/L_{HO2}}{c} \left(\frac{1}{\tau} - \frac{1}{\tau_0}\right) = \frac{1.17}{c} \left(\frac{1}{\tau} - \frac{1}{\tau_0}\right), \quad \text{(S6)}$$

The fit of Eq. (S5) to the experimental temporal decays of α_{HO2} computed using Eq. (S6) yielded the results shown in Table S5. The averaged values of the parameters are: $\sigma_{HO2} = (1.18 \pm 0.22) \times 10^{-19}$ cm^2 molecule^{-1} and $k_{loss} = (0.11 \pm 0.01)$ s^{-1}. It can be concluded that the use of the factor of 1.17 results in a change in σ_{HO2} within its overall 1σ error and does not change k_{loss}.

Table S5. Absorption cross section at 1506.43 nm, σ_{HO2}, and the rate coefficient of the HO_2 wall-loss, k_{loss}, extracted by fitting Eq. (S5) to the experimental α_{HO2} vs. time data at 150 mbar. α_{HO2} was computed using Eq. (S6), which provided 1.17 times higher values than the values of α_{HO2} calculated using Eq. (S4).

$10^{19} \times \sigma_{HO2}$[a] / cm^2 molecule^{-1}	k_{loss} / s^{-1}
1.19 ± 0.04[b]	0.109 ± 0.004
1.21 ± 0.04[b]	0.106 ± 0.005
1.12 ± 0.05[b]	0.102 ± 0.005
1.26 ± 0.04[b]	0.104 ± 0.004
1.21 ± 0.03[b]	0.110 ± 0.003
1.06 ± 0.07[c]	0.106 ± 0.007
1.25 ± 0.16[c]	0.109 ± 0.009

[a] uncertainties quoted to 1σ
[b] $[HO_2]_0$ = (1.30 ± 0.08) × 10^{11} molecule cm^{-3} (obtained by using: $[HO_2]_0 = (\alpha_{HO2})_0 / \sigma_{HO2}$)
[c] $[HO_2]_0$ = (5.22 ± 0.20) × 10^{10} molecule cm^{-3} (computed by using: $[HO_2]_0 = (\alpha_{HO2})_0 / \sigma_{HO2}$)

S9.3 σ_{HO2} (1506.43 nm) at 1000 mbar using the kinetics of the HO_2 temporal decay

In order to improve the precision of the σ_{HO2} determination at 1000 mbar, the FAGE signal decays recorded at the same time with the α_{HO2} decays were used to determine σ_{HO2}. The fluorescence signal decays were scaled to overlap α_{HO2} vs. time by multiplying the FAGE signal with $f = \frac{(\bar{\alpha}_{HO_2})_0}{(\bar{S}_{HO_2})_0}$, where $(\bar{\alpha}_{HO_2})_0$ and $(\bar{S}_{HO_2})_0$ are the average absorption coefficient and the mean FAGE signal before the UV lamps are switched off. Equation (S5), where the overall HO_2 self-reaction rate coefficient $k_{self\text{-}r.}$ was fixed to 2.85 × 10^{-12} cm^{-3} molecule^{-1} s^{-1} (Atkinson et al., 2004), was fitted to the scaled signal decays to obtain σ_{HO2} and k_{loss}. Six determinations were carried out in total with the results shown in Table S6; the average results are: σ_{HO2}(FAGE) = (3.87 ± 0.11) × 10^{-20} cm^2 molecule^{-1} and k_{loss}(FAGE) = (0.045 ± 0.004) s^{-1} (the error limits represent the standard errors generated by the fitting using Eq. (S5)).

The scaled FAGE signal decays were employed to determine σ_{HO2} as the scaled S_{HO2} decays overlapped very well with the α_{HO2}(1000 mbar) vs. time measurements (Figure 6 in the main manuscript shows an example). In addition, the analysis of α_{HO2}(1000 mbar) vs. time using Eq. (S5) provided an average σ_{HO2}(CRDS) = (3.68 ± 0.69) × 10^{-20} cm^2 molecule^{-1} (Table S6) in very good agreement with σ_{HO2}(FAGE). The average rate coefficient of the wall-loss was k_{loss}(CRDS) = (0.076 ± 0.028) s^{-1} and, hence k_{loss}(CRDS) and k_{loss}(FAGE) have overlapping error limits. The standard errors in the fit to the CRDS data were much higher than the standard errors in the fit to the scaled FAGE data: 19% associated

with σ_{HO2}(CRDS), compared to the only 3% fit precision in σ_{HO2}(FAGE) and 37% associated with k_{loss}(CRDS) compared to the ~ 4 times lower fit precision in k_{loss}(FAGE) (10%).

Table S6. σ_{HO2}(1506.43 nm) and the wall-loss rate coefficient within HIRAC, k_{loss}, at 1000 mbar obtained by fitting Eq. (S5) to: (i) the temporal decays obtained by multiplying the FAGE signal, $\left(S_{HO_2}\right)_t$, with $f = \frac{\left(\bar{\alpha}_{HO_2}\right)_0}{\left(\bar{S}_{HO_2}\right)_0}$, where $\left(\bar{\alpha}_{HO_2}\right)_0$ and $\left(\bar{S}_{HO_2}\right)_0$ are the average absorption coefficient and the mean FAGE signal before the UV lamps are extinguished and (ii) α_{HO2}(150 mbar) vs. time.

$10^{20} \times \sigma_{HO2,\ FAGE}$[a] / cm^2 molecule^{-1}	$k_{loss,\ FAGE}$[a] / s^{-1}	$10^{20} \times \sigma_{HO2,\ CRDS}$[a] / cm^2 molecule^{-1}	$k_{loss,\ CRDS}$[a] / s^{-1}
3.65 ± 0.04[b]	0.046 ± 0.004	3.89 ± 0.52[b]	0.08 ± 0.01
3.54 ± 0.06[b]	0.029 ± 0.008	3.47 ± 0.47[b]	0.07 ± 0.02
3.29 ± 0.05[b]	0.028 ± 0.002	4.30 ± 0.26[b]	0.07 ± 0.02
4.08 ± 0.06[b]	0.034 ± 0.005	3.27 ± 0.68[b]	0.08 ± 0.03
4.30 ± 0.30[c]	0.070 ± 0.011	3.69 ± 0.63[c]	0.01 ± 0.01
4.36 ± 0.13[c]	0.062 ± 0.004	3.49 ± 1.56[c]	0.14 ± 0.07

[a] uncertainties quoted to 1σ
[b] $[HO_2]_0$ ~ 1 × 10^{10} molecule cm^{-3} (obtained by using: $[HO_2]_0 = (\alpha_{HO2})_0 / \sigma_{HO2}$)
[c] $[HO_2]_0$ between (6 – 7) × 10^{10} molecule cm^{-3} (computed by using: $[HO_2]_0 = (\alpha_{HO2})_0 / \sigma_{HO2}$)

S10 Intercomparison of CRDS and FAGE HO_2 measurements

In some intercomparison experiments the lamps were alternately turned on for 2–3 min and then off for ~ 3 min to generate a series of typically three HO_2 temporal decays followed by regeneration of the HO_2 (Figs. S7 and S8).

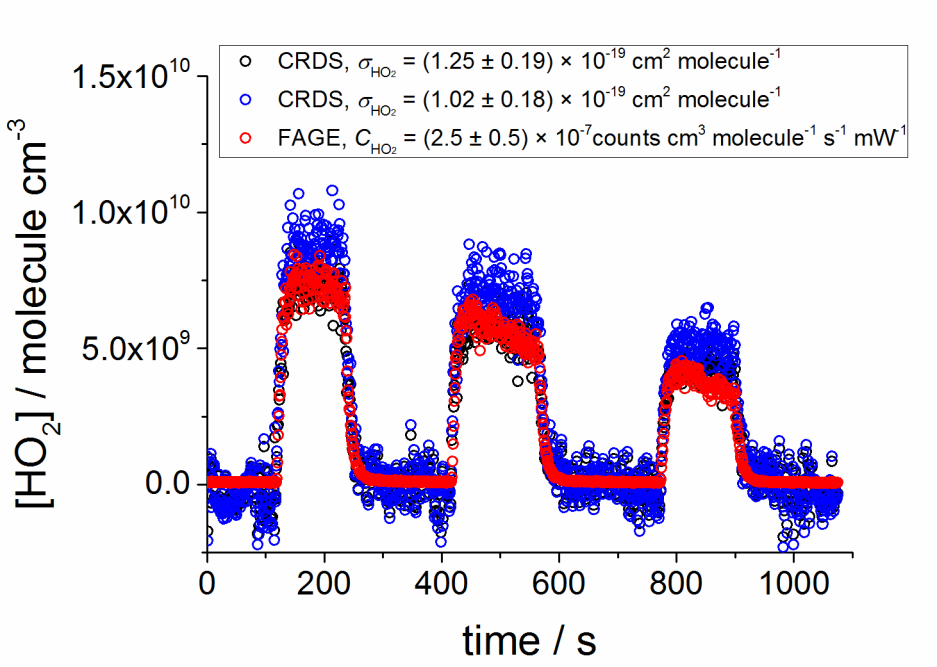

Figure S7. Comparison measurement at 150 mbar where the lamps were alternatively turned on and then off, every time for 100–200 s. [HO_2] was computed using a FAGE calibration factor C_{HO2} = 2.6 × 10^{-7} counts cm^3 molecule^{-1} s^{-1} mW^{-1} (red) and a cross section at 1506.43 nm σ = 1.25 × 10^{-19} cm^2 molecule^{-1} (black) and σ = 1.02 × 10^{-19} cm^2 molecule^{-1} (blue) - details in the main paper. Data averaged over 1 sec. Concentrations at time zero: [CH_3OH]$_0$ = 6.6 × 10^{13} molecule cm^{-3}, [Cl_2]$_0$ = 7.1 × 10^{12} molecule cm^{-3}.

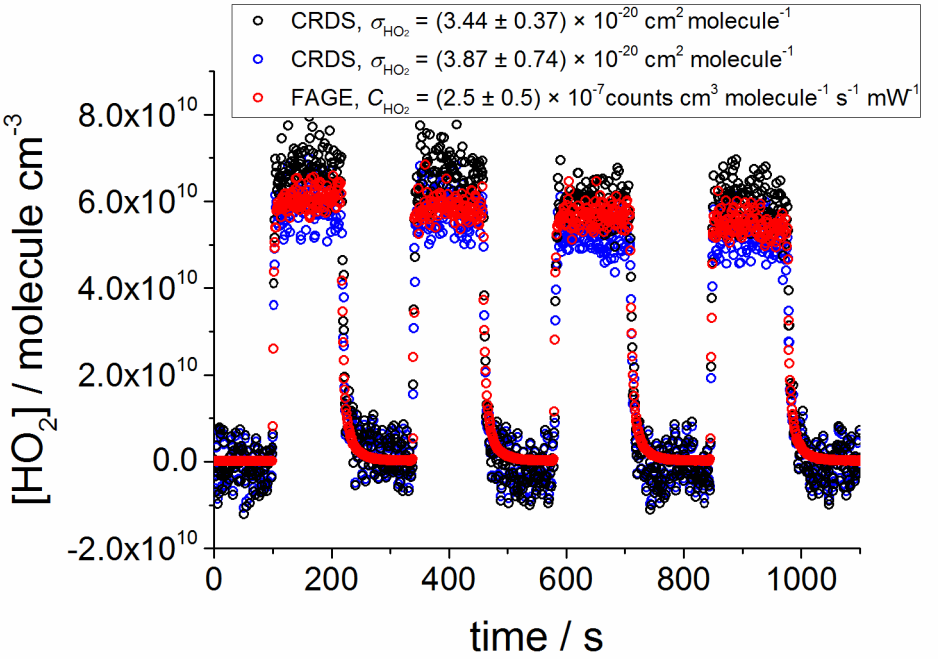

Figure S8. Comparison measurement at 1000 mbar where the lamps were alternatively turned on and then off, every time for 100–200 s. [HO_2] was computed using the FAGE calibration factor obtained by averaging the values determined by the two calibration methods, the H_2O photolysis and the kinetics of the HO_2 decays, $C_{1000\ mbar}$ = 2.5 × 10^{-7} counts cm^3 molecule^{-1} s^{-1} mW^{-1} (red) and a cross section at 1506.43 nm σ = 3.44 × 10^{-20} cm^2 molecule^{-1} (black) and σ = 3.87 × 10^{-20} cm^2 molecule^{-1} (blue)) - details in the main paper. Data averaged over 1 sec. Concentrations at time zero: [CH_3OH]$_0$ ~ 8 × 10^{13} molecule cm^{-3}, [Cl_2]$_0$ ~ 4 × 10^{13} molecule cm^{-3}.

References

Atkinson, R., Baulch, D. L., Cox, R. A., Crowley, J. N., Hampson, R. F., Hynes, R. G., Jenkin, M. E., Rossi, M. J., and Troe, J.: Evaluated kinetic and photochemical data for atmospheric chemistry: Volume I - gas phase reactions of Ox, HOx, NOx and SOx species, Atmospheric Chemistry and Physics, 4, 1461-1738, 2004.

Glowacki, D. R., Goddard, A., Hemavibool, K., Malkin, T. L., Commane, R., Anderson, F., Bloss, W. J., Heard, D. E., Ingham, T., Pilling, M. J., and Seakins, P. W.: Design of and initial results from a Highly Instrumented Reactor for Atmospheric Chemistry (HIRAC), Atmos. Chem. Phys., 7, 5371-5390, 2007.

Richard, C., Gordon, I. E., Rothman, L. S., Abel, M., Frommhold, L., Gustafsson, M., Hartmann, J. M., Hermans, C., Lafferty, W. J., Orton, G. S., Smith, K. M., and Tran, H.: New section of the HITRAN database: Collision-induced absorption (CIA), J. Quant. Spectrosc. Ra., 113, 1276-1285, 10.1016/j.jqsrt.2011.11.004, 2012.

Ruth, A. A., Heitmann, U., Heinecke, E., and Fittschen, C.: The Rotationally-Resolved Absorption Spectrum of Formaldehyde from 6547 to 7051 cm^{-1}, Z. Phys. Chem. , 229, 1609-1624, 10.1515/zpch-2015-0623, 2015.

Winiberg, F. A. F., Dillon, T. J., Orr, S. C., Gross, C. B. M., Bejan, I., Brumby, C. A., Evans, M. J., Smith, S. C., Heard, D. E., and Seakins, P. W.: Direct measurements of OH and other product yields from the HO_2 +$CH_3C(O)O_2$ reaction, Atmos. Chem. Phys., 16, 4023-4042, 2016.